Multiscale Variability of the Atmospheric Boundary Layer during DYNAMO

RICHARD H. JOHNSON AND PAUL E. CIESIELSKI

Department of Atmospheric Science, Colorado State University, Fort Collins, Colorado

(Manuscript received 14 June 2017, in final form 12 September 2017)

ABSTRACT

Properties of the atmospheric boundary layer (ABL) over the central Indian Ocean are investigated using sounding data obtained during the Dynamics of the MJO (DYNAMO) field campaign in 2011/12. Observations from Gan Island on Addu Atoll, the R/V *Revelle*, and Malé in the Maldives are used to determine the frequency of well-mixed layers and their mean thermodynamic and wind profiles. Well-mixed boundary layers or mixed layers were observed 68% of the time from the three sites, ranging from ~100-m depth in recovering convective downdraft wakes to ~925 m in undisturbed conditions, with a mean depth of 508 m. At *Revelle*, the site most representative of the open ocean, the ABL displayed a distinct signal of modulation by the October and November MJOs, with mixed-layer depths gradually increasing through the suppressed phases as the sea surface temperature (SST) increased leading up to the active phases, followed by frequent ABL stabilization and shallow mixed layers in recovering wakes. A distinct diurnal cycle of mixed-layer depths and properties was observed during the MJO suppressed phases in response to a diurnal cycle of the SST under the mostly light-wind, clear-sky conditions. The daytime growth of the mixed layer contributed to an afternoon maximum in cumulus cloud development and rainfall during the suppressed periods by allowing more boundary layer thermals to reach their condensation levels. The variability of the ABL on time scales ranging from convective to diurnal to monthly poses significant challenges for numerical simulations of the MJO and the tropical circulation in general.

1. Introduction

A major challenge in numerical weather and climate prediction is the realistic treatment of the atmospheric boundary layer (ABL) (Teixeira et al. 2008). Complicating factors include the coupling of the boundary layer with the underlying surface, stratification effects, surface inhomogeneities, complex turbulent structures, intermittency, and nonlocal mixing. An additional difficulty, particularly in the tropics, is the coupling of the ABL with the cloud layer, including boundary layer modification by convective clouds and precipitation. The challenge extends well beyond individual clouds to organized convective systems across a wide span of time scales, from mesoscale convective systems to equatorial waves to the Madden–Julian oscillation (MJO). The recent Dynamics of the MJO (DYNAMO)[1] field campaign (Yoneyama et al. 2013; Zhang et al. 2013) affords a unique opportunity to investigate the multiscale variability of the boundary layer under a wide range of convective activity throughout the life cycle of the MJO.

Surface, sounding, and radar measurements collected during DYNAMO have shed new light on properties of the boundary layer and lower troposphere from the suppressed to active phases of the MJO. During suppressed periods, boundary layer circulations frequently developed that brought about organized roll and cellular patterns of shallow convection and played a role in

Corresponding author: Richard H. Johnson, johnson@atmos.colostate.edu

[1] The field campaign consisted of four collaborating components: DYNAMO, Cooperative Indian Ocean Experiment on Intraseasonal Variability in the Year 2011 (CINDY), ARM MJO Investigation Experiment (AMIE), and Littoral Air-Sea Processes (LASP). We will refer to the combined effort as DYNAMO.

DOI: 10.1175/JAS-D-17-0182.1

lower-tropospheric moistening (Bellenger et al. 2015; Rowe and Houze 2015; Ruppert and Johnson 2015, 2016). Despite the shallowness and scattered nature of convection during these times, evaporation from precipitating clouds generated distinct cold pools that modified near-surface wind and thermodynamic conditions (Chen et al. 2016; de Szoeke et al. 2017), contributing to further convective cloud development (Rowe and Houze 2015; Feng et al. 2015). Proceeding into the active phase, the frequency of cold pools increased (Moum et al. 2014; de Szoeke et al. 2017) associated with increased rainfall and more numerous mesoscale convective systems (Xu and Rutledge 2014). The characteristics of the convectively generated cold pools over the Indian Ocean during DYNAMO bear close resemblance to those previously observed in field campaigns over the tropical Atlantic (Houze 1977; Zipser 1977; Barnes and Garstang 1982; Johnson and Nicholls 1983; Jorgensen et al. 1997; Zuidema et al. 2012) and the tropical western Pacific (Young et al. 1995; Saxen and Rutledge 1998).

While the evolution of surface wind and thermodynamic properties, surface fluxes, upper-ocean structure, clouds, and precipitation fields over the life cycle of the DYNAMO MJOs have been documented in a number of recent studies (Johnson and Ciesielski 2013; Powell and Houze 2013, 2015b; Moum et al. 2014; Xu and Rutledge 2014; de Szoeke et al. 2015, 2017; Baranowski et al. 2016), the variability of the atmospheric mixed layer during DYNAMO has yet to be fully explored. In an investigation for a limited period of DYNAMO, Chen et al. (2016) found using aircraft dropsonde data that the height of the atmospheric boundary layer was ~100 m greater during the suppressed phase of the November DYNAMO MJO than during the convectively active phase. This observation is consistent with the findings of Johnson et al. (2001), who used sounding data from the Tropical Ocean and Global Atmosphere Coupled Ocean–Atmosphere Response Experiment (TOGA COARE) to investigate the multiscale variability of the mixed layer for that experiment. It was found that well-mixed layers were observed about two-thirds of the time during COARE, ranging from as high as 960-m depth during periods of dry intrusions over the warm pool to as shallow as ~100–200 m in recovering downdraft wakes. In addition, a diurnal variation in the mixed-layer depth was observed on undisturbed, light-wind days during the suppressed phase of the December 1992 MJO when a diurnal cycle in sea surface temperature (SST) up to 2°–3°C existed.

It is becoming increasingly clear that a realistic representation of the boundary layer throughout the life cycle of the MJO is important for successful numerical simulations of the phenomenon. The sensitivity of simulations of the MJO to the treatment of the boundary layer was recently demonstrated by Qian et al. (2016), who showed using the Weather Research and Forecasting (WRF) Model that the simulated precipitation and surface moisture fluxes over the Indian Ocean during DYNAMO exhibited "surprising large" differences with the application of various boundary layer parameterization schemes. These authors compared simulated boundary layer properties to those observed by soundings taken at Addu Atoll (Gan Island) and found significant differences in the profiles of virtual potential temperature, moisture, and moist static energy extending from the surface up to 5 km for the different boundary layer schemes used.

A further complication to boundary layer treatment in MJO simulations is the proper representation of diurnal cycle effects. A substantial diurnal cycle in SST was observed during the DYNAMO suppressed phases (Matthews et al. 2014; Chen et al. 2015; Ruppert and Johnson 2015), which presumably impacts the diurnal cycle of the atmospheric mixed layer, as was shown to be the case for COARE (Johnson et al. 2001). The SST diurnal cycle appears to be important for realistic model representation of lower-tropospheric moistening during the preonset phase of the MJO (Seo et al. 2014; Ruppert and Johnson 2016).

The present study aims to utilize the extensive DYNAMO sounding dataset to determine the multiscale variability of the atmospheric mixed layer over the Indian Ocean during that experiment and compare the findings to those for COARE reported in Johnson et al. (2001). There are several advantages of the DYNAMO dataset over COARE for study of the mixed layer. First, there were three prominent MJOs during DYNAMO (in October, November, and December) as opposed to a single distinct event in COARE. Second, the higher time resolution of soundings (3 hourly) during DYNAMO is superior for determining the diurnal cycle of the mixed layer than the 6-hourly soundings during COARE. Finally, there have been significant improvements in the radiosonde humidity sensors used during DYNAMO over those used 20 yr earlier in COARE such that humidity sensor errors have been much reduced (Ciesielski et al. 2014).

2. Data and methods

a. Data

Mixed-layer properties are determined from the radiosonde measurements taken from the DYNAMO sounding arrays. The DYNAMO sounding network consisted of two quadrilateral arrays: one north and one

south of the equator (Fig. 1). Details of the sounding systems, observing characteristics, and sounding data quality-control procedures are contained in Ciesielski et al. (2014). As indicated by the MJO amplitude shown in Fig. 1 and reported in Johnson and Ciesielski (2013), the strongest MJO signal occurred over the northern sounding array, as opposed to the southern array. Therefore, for the purposes of this study, mixed-layer properties are examined at the three sites—Gan Island, Malé, and the R/V *Revelle*—in Fig. 1. Soundings from Malé were at 6-hourly intervals, while those at Gan and *Revelle* were at 3-hourly intervals. The October–November period of DYNAMO was designated the special observing period (SOP); however, the sounding arrays were intact for the majority of the time between 1 October and 15 December, so we will refer to the latter period as the SOP. Soundings from Colombo, Sri Lanka, were heavily influenced by local island effects, so that site is excluded from the mixed-layer analysis.

Soundings at Gan Island, Malé, and *Revelle* used Vaisala RS92 systems. The humidity data have been corrected following the procedures outlined in Ciesielski et al. (2014). The corrected RS92 humidity data had a slight nighttime moist bias (~1%) in the lower troposphere, considerably less than that of the RS80 sensors used in COARE. Surface data points for the soundings were from meteorological sensors at 2 m at Gan Island and Malé and 19 m at *Revelle*.

Surface fluxes and SST were obtained from in situ measurements on board the R/V *Revelle*, made available via ftp://dynamo.dms.uconn.edu/ through a collaborative effort between NOAA/ESRL/Physical Sciences Division, Oregon State University, and the University of Connecticut. Bulk fluxes were computed using the COARE 3.0 algorithm (Fairall et al. 2003).

Rainfall rates at Gan and *Revelle* are based on the National Center for Atmospheric Research (NCAR) S-band/Ka-band Dual Polarization, Dual Wavelength Doppler Radar (S-PolKa) and Tropical Ocean Global Atmosphere (TOGA) radar estimates, respectively, obtained from the DYNAMO Data Legacy Project website at http://dynamo.fl-ext.ucar.edu/rsmas/dynamo_legacy/. The radar estimates for Gan and *Revelle* are 10-min averages over a 320 km × 320 km area surrounding each site. Images of PPI scans from the TOGA radar aboard the *Revelle* are from http://catalog.eol.ucar.edu/dynamo/. *Terra*/MODIS satellite images have been obtained from https://lance3.modaps.eosdis.nasa.gov/cgi-bin/imagery/realtime.cgi. Rainfall at the three sites was also estimated from the 3-h, 0.25° resolution TRMM 3B42v7 rainfall product (Huffman et al. 2007). Cloud-cover estimates were based on ceilometer observations at *Revelle*. Cloud coverage for the November suppressed period was defined from 1-h ceilometer data as the fraction of the time clouds were overhead. Vertical motion field used in constructing Fig. 1 was from the V3b Colorado State University gridded analysis product at http://johnson.atmos.colostate.edu/dynamo/products/gridded/index.html.

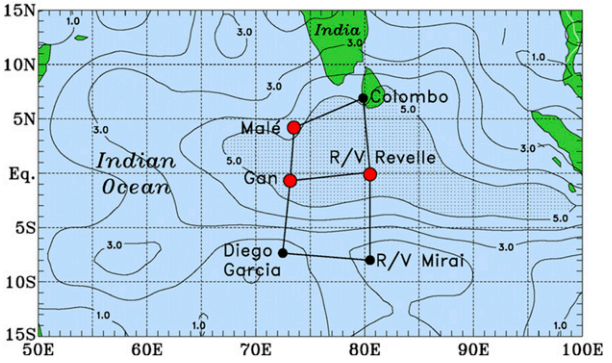

FIG. 1. DYNAMO enhanced sounding network for the period October–December 2011. Analyses of mixed layers have been carried out on soundings from Malé (4 day^{-1}), Gan Island (8 day^{-1}), and *Revelle* (8 day^{-1}) (red dots), which constituted part of the northern sounding array. That array experienced a stronger MJO signal than the southern array as indicated by amplitude of 20-day low-pass-filtered 450-hPa vertical motion (contours; hPa h^{-1}, values >5 hPa h^{-1} are stippled). Colombo data were not used because of significant island influences.

b. *Mixed-layer depth analysis*

Mixed layers are commonplace over the tropical ocean, characterized by a layer ~500–600 m deep of nearly constant potential temperature θ (e.g., Malkus 1958; LeMone and Pennell 1976; Fitzjarrald and Garstang 1981; Johnson et al. 2001). Specific humidity q in mixed layers ranges from being a constant to gradually decreasing with height through its depth by 0.5–1 g kg^{-1}. This decrease is a result of dry-air entrainment into the mixed layer, as reflected by large variances in q in the upper part of the mixed layer (e.g., Nicholls and LeMone 1980). The mixed layer is typically capped by an entrainment zone ~50–150 m deep containing sharp vertical gradients in θ and q. During periods of precipitation, cool downdraft outflows often stabilize the boundary layer, followed by a recovery period with deepening mixed layers lasting from a few hours up to a half day or longer (e.g., Zipser 1977; Young et al. 1995; Jorgensen et al. 1997; Chen et al. 2016).

A variety of objective techniques have been developed to determine the depth of the atmospheric boundary layer (ABL) under stratifications ranging from convectively unstable, to neutral, to stable. Mixed layers commonly exist under unstable and neutral conditions. The techniques used, however, often lead

to different ABL and mixed-layer depth estimates (e.g., Liu and Liang 2010; Seidel et al. 2010; Wang and Wang 2014). Recognizing these difficulties and drawing upon experience from COARE (Johnson et al. 2001), we use the subjective procedure employed in that study for identification of mixed layers and determination of their depths and properties, which is described next.

Soundings from Malé, Gan, and *Revelle* (Fig. 1) are identified as having mixed layers if the following conditions are met: θ is approximately constant with height from the surface (or the top of a superadiabatic layers when it exists) up to a height z_i, the mixed-layer top, with an abrupt increase in stability above z_i, and q is constant or decreases only slightly from the surface up to z_i and then decreases rapidly above. The vertical resolution of the sounding data used in the analysis is 5 hPa, which roughly corresponds to 50 m in the boundary layer. Since the true z_i may not correspond exactly with one of the 5-hPa pressure levels, a sounding is designated as having a mixed layer if it is determined that a mixed layer exists for both θ and q and the values of z_i for each agree within 5 hPa of each other. The value of z_i assigned for the sounding is based on which θ or q profile best depicts a well-mixed structure. An entrainment zone ~50–150 m deep having a base at z_i was observed for many of the mixed layers. Although the top of the entrainment zone was not determined in our analysis, its existence shows up in plots of the thermodynamic properties of mixed layer scaled by mixed-layer depth that are presented later.

A complication with determination of mixed-layer properties from Gan and Malé is the fact that the soundings were taken over land adjacent to airport runways. Given the well-known heating effect of islands (e.g., Malkus and Stern 1953), the lowest part of soundings is often modified from the structure that exists over the adjacent open ocean. The Malé observation site was on Velana International Airport portion of Hulhule Island, a strip of land approximately 500 m wide and 3000 m long. The Gan observation site was on Addu Atoll, a much larger island with an enclosed shallow lagoon approximately 5 km across. The heat source represented by Addu Atoll clearly has the potential to influence the boundary layer properties given by the Gan soundings. The smaller dimension of Malé compared with Gan argues for a smaller heat-island effect there; nevertheless, land effects cannot be ignored in the interpretation of the lowest 50 m of the Malé soundings. The soundings from *Revelle* are the most representative of open-ocean conditions, but the ship superstructure no doubt impacted the lowest 50 m or so for some of the soundings.

3. Results

a. Mean properties of the mixed layer

The focus of the study is on well-mixed boundary layers, which can occur under unstable or neutral conditions. Characteristics of stable layers, other than their frequency of occurrence, are not considered here. Two instances where mixed layers were identified are illustrated in Fig. 2, which is a plot of soundings from the *Revelle* taken on 4 October during the suppressed phase of the MJO. Profiles of θ and q are approximately well mixed up to about 500 m, surmounted by an entrainment zone ~100 m deep featuring sharp increases in stability and strong drying. Although not the focus of our study, the figure depicts a hypothesized trade wind–like cumulus layer, capped by a slightly more stable layer and increased moisture lapse rate (Malkus 1958; Augstein et al. 1974). This illustration provides a broader context for the types of conditions observed during the suppressed phases of the MJO. In support of this depicted structure, the *Terra*/MODIS visible image in Fig. 2 shows scattered cumulus patches in the area of the *Revelle* around the time of the soundings. Similar trade wind–like conditions during the suppressed phase of the MJO were observed during COARE (Johnson and Lin 1997).

As previously mentioned, an advantage of having 3-hourly soundings is the ability to better resolve the diurnal cycle of the mixed layer. However, this time resolution also allows for an improved sampling over that during COARE of the recovery of the mixed layer following deep convection. As an illustration, soundings at 3-hourly intervals from the *Revelle* on 22 November (Fig. 3) show the stabilization of the boundary layer around 0200 UTC [0700 local time (LT)] by precipitation systems detected by the TOGA radar at 0229 UTC. Over the following 12 h, the mixed layer deepened from 985 hPa (230 m) at 1000 LT (0500 UTC) to 970 hPa (360 m) at 1900 LT (1400 UTC) as the precipitation waned. This lengthy recovery period is consistent with some of the DYNAMO cases reported by Chen et al. (2016) using aircraft data to determine recovery times and is not unlike findings from past studies (Houze 1977; Zipser 1977; Fitzjarrald and Garstang 1981; Johnson and Nicholls 1983; Jorgensen et al. 1997).

An inventory of sounding classifications for all three sites is provided in Table 1. An average of 68% (ranging from 64% to 72%) of the 1783 soundings examined in DYNAMO exhibited mixed-layer structures, slightly less than the 72% reported by Johnson et al. (2001) for soundings analyzed in COARE. These percentages are also somewhat less than the 79.5% frequency of mixed layers that Fitzjarrald and Garstang (1981) determined

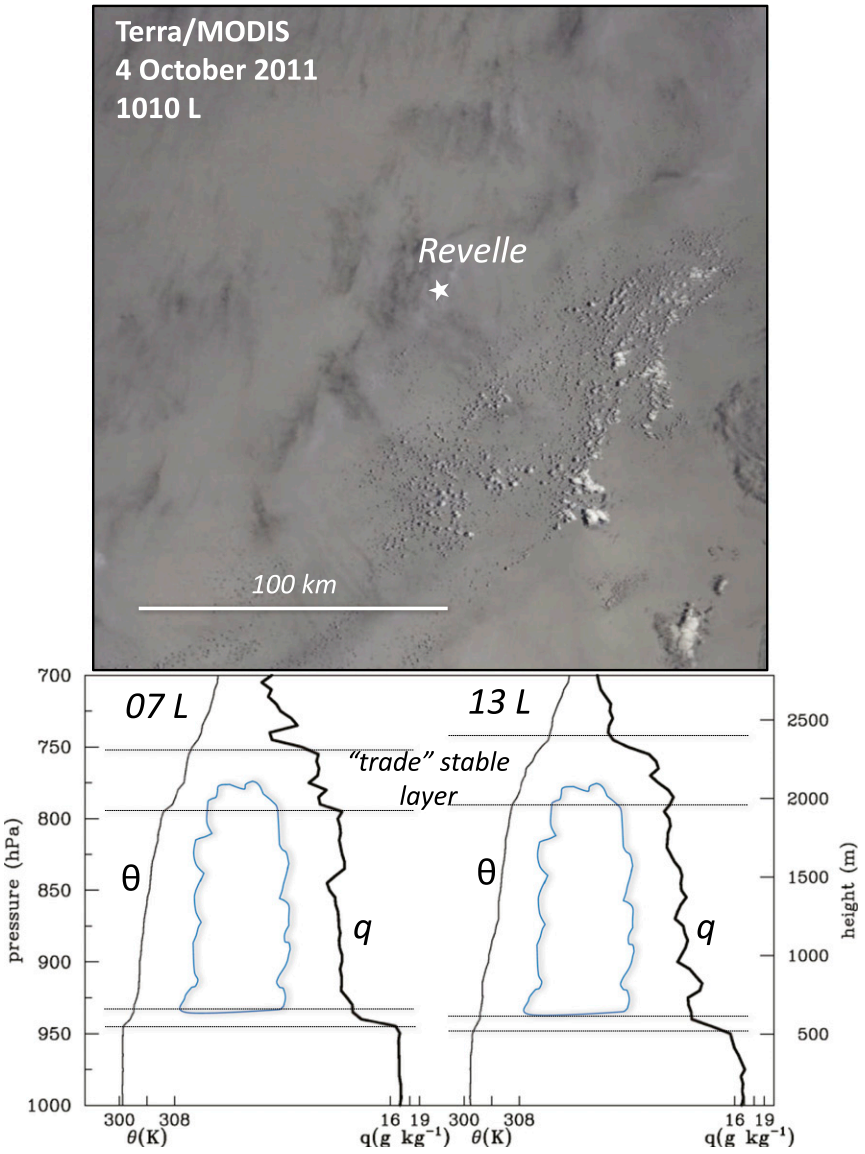

FIG. 2. (bottom) Potential temperature θ and specific humidity q profiles at 0700 and 1300 LT at R/V *Revelle* during a suppressed period of the MJO on 4 Oct 2011. Nearly well-mixed profiles of θ and q extend up to approximately 500 m, surmounted by a ~100-m-deep entrainment zone. Hypothesized cumulus cloud layer is depicted, topped by a trade wind–like stable layer. (top) *Terra*/MODIS visible image at 1010 LT indicates some scattered clouds in the region. Image extends from approximately 1° to 2°S and from 80° to 81°E. Patchiness of sea surface is a result of image occurring in sun glint. Star denotes approximate position of *Revelle*.

using the Boundary Layer Instrumentation System in the GARP Atlantic Tropical Experiment (GATE). Table 1 shows that stable layers, which principally occurred during periods of precipitation, existed on average about 12% of the time, while the remaining soundings (17%) had indeterminate profiles; that is, they were not stable, but a well-mixed structure could not be identified.

Mean properties of the mixed layers at the three sites for the SOP are shown in Table 2, along with comparisons with COARE and GATE results. The mean mixed-layer depth $\overline{z}_i$ for the three sites in DYNAMO is 508 m. The ranking of mean depths from highest to lowest, from 535 m at Malé to 503 m at Gan to 491 m at *Revelle*, is the reverse of the ranking of rainfall rates and frequency of rainfall at the three sites (Table 2). Namely, shallower mean mixed-layer depths occurred with the greater rainfall rates and rainfall frequencies, implying the more frequent recovering precipitation downdraft wakes. The

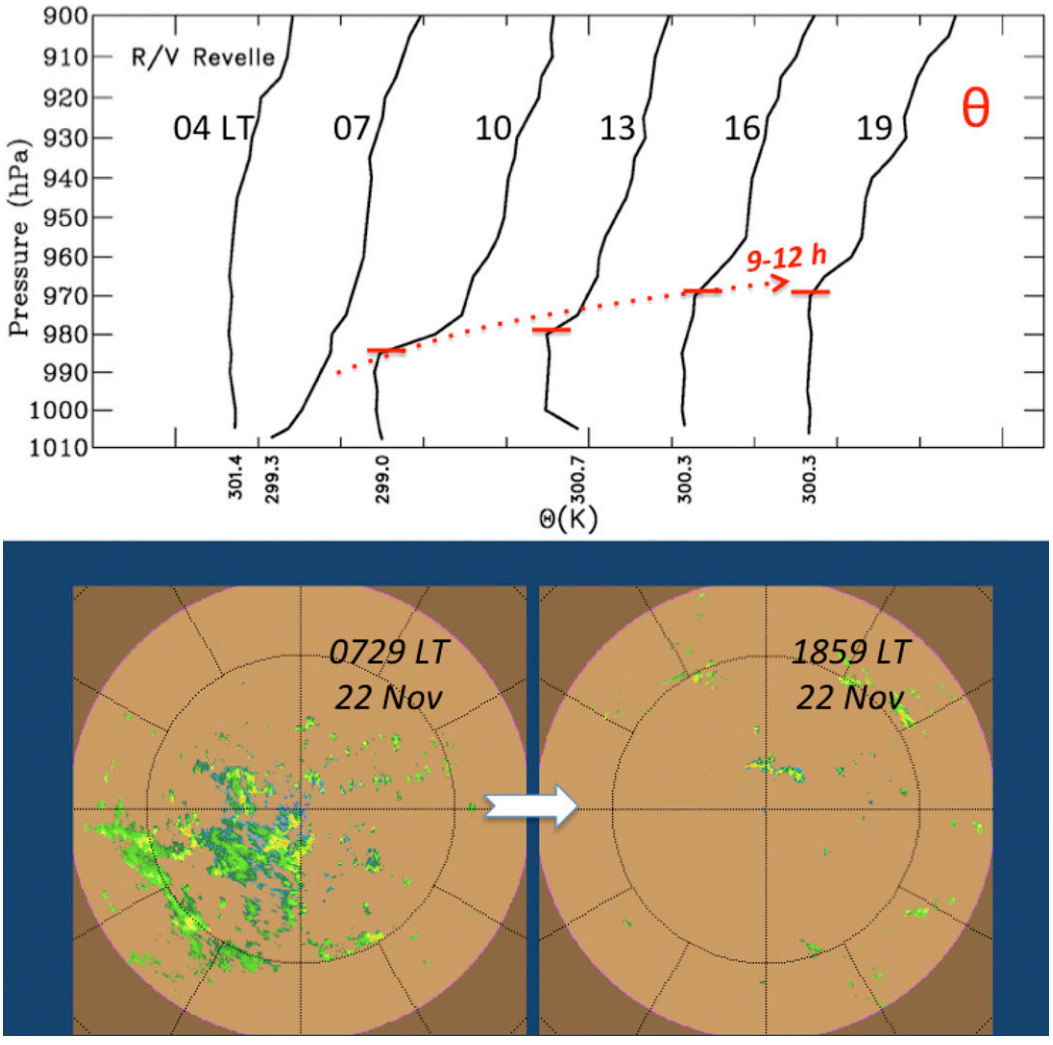

FIG. 3. (top) Sequence of potential temperature θ profiles at R/V *Revelle* from 2300 UTC 21 Nov to 1400 UTC 22 Nov (local times at 3-h intervals indicated along θ profiles within panel). Boundary layer recovery (mixed-layer tops indicated by red line segments) over a 12-h period is approximated by dashed arrow. Surface θ values indicated at base of each sounding. Successive soundings are separated by 3 K. (bottom) Radar reflectivity PPI scans from TOGA radar (out to 150-km radius) at 0729 and 1859 LT showing decrease in areal coverage of precipitation systems. Reflectivity range is from 20 (dark green) to 45 dBZ (orange).

large standard deviations (146–171 m) of z_i reflect the existence of numerous mixed-layer modifying processes: convective downdrafts from isolated showers all the way up to mesoscale convective systems, westerly wind bursts, organized boundary layer circulations such as rolls and open cells, and the diurnal cycle. The mean z_i of 508 m

TABLE 1. Boundary layer statistics for Gan Island for 1 Oct 2011–8 Feb 2012, and Malé and R/V *Revelle* for 1 Oct–15 Dec 2011, and comparisons with TOGA COARE (Johnson et al. 2001) and GATE (Fitzjarrald and Garstang 1981). Numbers in parentheses are percentages of cases. Soundings with bad or missing data in ABL have been excluded from the DYNAMO sounding inventory.

	Sounding site					
	Gan Island	Malé	R/V *Revelle*	DYNAMO totals	TOGA COARE	GATE
Number of sondes	1049	316	418	1783	1283	703
Mixed-layer cases	726 (69.2%)	226 (71.5%)	268 (64.1%)	1220 (68.4%)	926 (72.1%)	559 (79.5%)
Stable-layer cases	105 (10.0%)	36 (11.4%)	59 (14.1%)	200 (11.6%)	—	—
Indeterminate cases	200 (19.1%)	54 (17.1%)	57 (13.6%)	311 (17.4%)	—	—

TABLE 2. Mean mixed-layer and rainfall statistics for Gan Island, Malé, and R/V *Revelle* during special observing period (1 Oct–15 Dec 2011), and comparisons with TOGA COARE (Johnson et al. 2001) and GATE (Fitzjarrald and Garstang 1981). Rainfall is from TRMM averaged within a 1° radius of each site. Sigma (σ) refers to standard deviation.

Station	Number	$\overline{z}_i$ (m)	σ (m)	Skewness	z_{max}	z_{min}	Rainfall rate (mm day^{-1})	Rainfall frequency (%)
Gan Island	396	503	146	−0.3	867	111	7.6	61
Malé	226	535	171	−0.01	926	165	5.6	53
Revelle	268	491	165	−0.1	914	132	9.1	65
DYNAMO total	890	508	158	−0.2	926	111	8.5	62
TOGA COARE	926	512	155	0.1	961	116	8.2[a]	—
GATE	703	424	160	—	—	—	—	—

[a] Mean rainfall rate in intensive flux array for intensive observing period of TOGA COARE (Johnson and Ciesielski 2000).

for DYNAMO is in close agreement with the 512-m mean value for COARE (Johnson et al. 2001) based on a nearly equal number of cases but is somewhat greater than the GATE mean value of 424 m obtained by Fitzjarrald and Garstang (1981).

Histograms of mixed-layer depths (Fig. 4) show similar distributions and a wide range of values at all sites during DYNAMO. Using a chi-square test, the distributions are found to be normal or Gaussian at the 0.05 significance level. However, each has negative skewness, reflecting the effects of convective downdraft wakes and shallow mixed layers during the recovery process. To illustrate the role of precipitation influence on mixed-layer depth, a histogram of mixed-layer depths for undisturbed and disturbed periods using the full record of soundings (1 October–8 February) at Gan during DYNAMO is shown in Fig. 5. Undisturbed periods are defined according to Ruppert and Johnson (2015) as suppressed and "bottom heavy" heating periods, while disturbed periods are defined as periods with "top

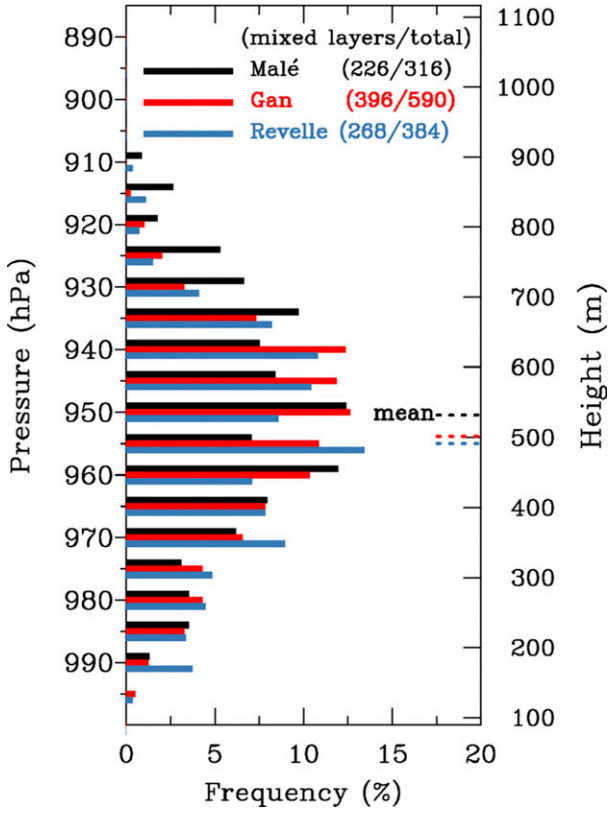

FIG. 4. Histograms of mixed-layer depth at Malé, Gan Island, and *Revelle* for the SOP (1 Oct–15 Dec) using 5-hPa bins. Horizontal dashed lines indicate mean values. Numbers of mixed-layer cases and total soundings during period are in parentheses.

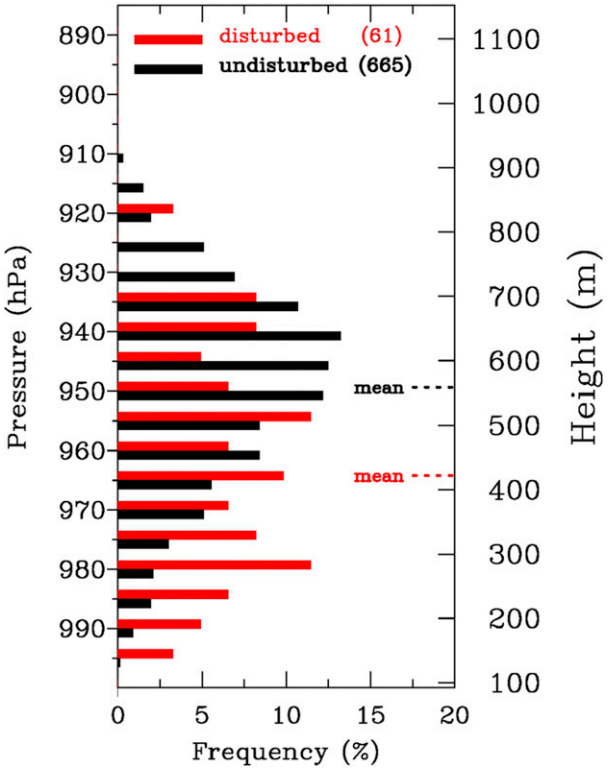

FIG. 5. Histograms of mixed-layer depth at Gan Island for undisturbed (black) and disturbed (red) periods for the full duration of DYNAMO (1 Oct 2011–8 Feb 2012) using 5-hPa bins. See text for definitions. Horizontal dashed lines indicate mean values. Numbers of mixed-layer cases are in parentheses.

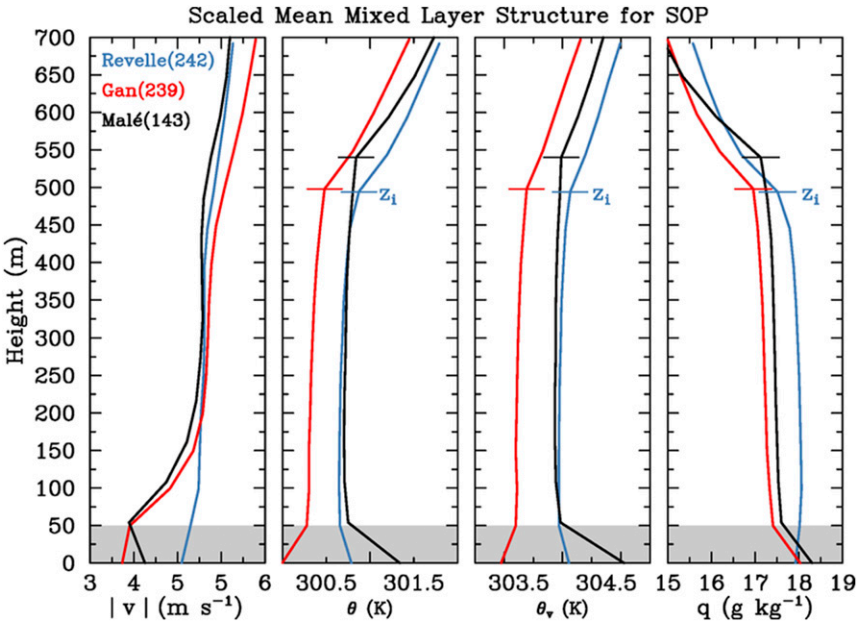

FIG. 6. SOP mean profiles of wind speed $|v|$, potential temperature θ, virtual potential temperature θ_v, and specific humidity q for *Revelle*, Gan, and Malé scaled by mixed-layer depth. Mean mixed-layer depths z_i for individual sites indicated by horizontal lines. Shading at bottom indicates surface effects in sounding data in lowest 50 m. Plots for all sites include only those times when *Revelle* was on station at its equatorial location (0800 UTC 3 Oct–0800 UTC 29 Oct and 2000 UTC 10 Nov–0800 UTC 1 Dec). Numbers of soundings indicated in parentheses.

heavy'' heating rates. This division of periods reflects the vertical growth of convection into the active phase of the MJO while at the same time a progression toward increasing areal coverage of convective downdrafts and their initially shallow but recovering wakes. There are stark differences in the distributions, with a single peak at upper levels on undisturbed days and several peaks (perhaps as a result of the smaller sample size) at lower levels on disturbed days. The mean z_i on undisturbed days is 559 m, while it is 422 m on disturbed days.

Figure 6 shows the mean wind and thermodynamic properties in the mixed layer for all three sites. To make the comparisons contemporaneous, soundings were included for only those times when the *Revelle* was on station at its equatorial location. To preserve mixed-layer structures, variables in each sounding are first scaled by mixed-layer depth z_i, then composited according to height relative to z_i, and finally replotted unscaled such that the mean values of z_i for each site are appropriately shown. Sounding data in the lowest 50 m are shaded to indicate a region of varying surface effects. Mean profiles of θ, virtual potential temperature θ_v, and q are nearly well mixed at all three sites, though θ is about 0.5 K cooler at Gan than at Malé or *Revelle*. Although data are not scaled relative to the depth of the entrainment zone, its existence is evident in most of the composite profiles by changes in stability and lapse rate of q ~50–100 m above z_i. It is unclear why Gan is slightly cooler than *Revelle*, in particular, since the latter location is slightly rainier (Table 1) and the mean SST during DYNAMO at all three sites is approximately the same (Johnson and Ciesielski 2013). Moreover, the Gan sounding site is along a runway, so it is not obvious why the mixed layer should be cooler there. With respect to q, the fact that *Revelle* is slightly moister makes sense since it is a rainier location. Wind speeds in the mixed layers are about the same throughout much of their depths (~5 m s^{-1}), though Gan and Malé are slightly calmer in the lowest 200 m owing to island/atoll frictional effects. The mixed-layer properties shown in Fig. 6 closely resemble those found by Fitzjarrald and Garstang (1981) for GATE and Johnson et al. (2001) for COARE.

To characterize the properties of the mixed layers more fully, contoured frequency by altitude diagrams (CFADs; Yuter and Houze 1995) of mixed-layer-mean θ, q, and TOGA radar rainfall within 3 h of sounding observation time at *Revelle* were constructed (Fig. 7). Shallow mixed layers were cooler and moister (higher q) than deep mixed layers as a result of precipitation downdrafts associated with higher rainfall rates. Deep mixed layers most often occurred under nonrainy conditions

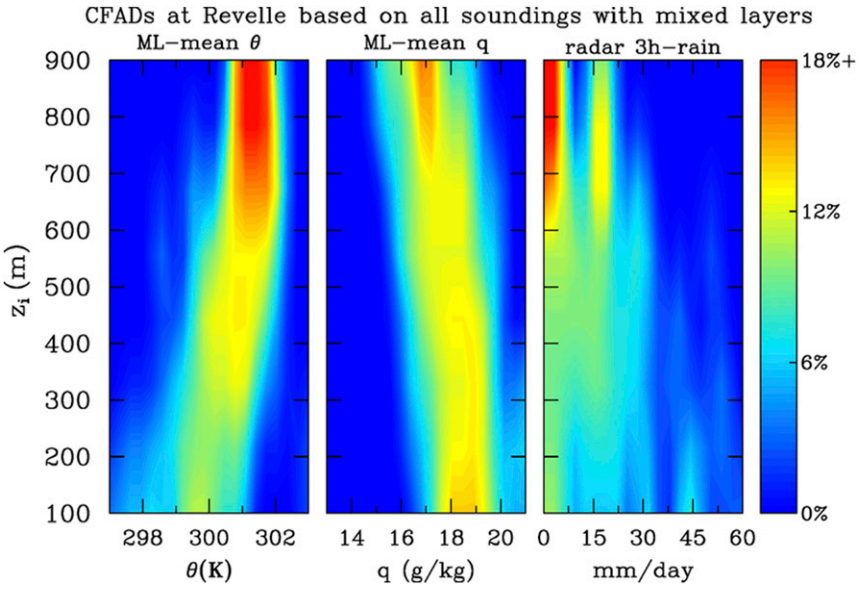

FIG. 7. CFADs of mixed-layer-mean θ, q, and radar rainfall at *Revelle* for 268 mixed-layer cases. Vertical axis is mixed-layer depth. Data have been placed into 20 bins in the horizontal and 8 bins in the vertical to create the CFADs. TOGA radar-estimated rainfall is for 3-h period centered on sounding observation times.

as indicated by radar-determined rainfall (except for an isolated peak near 20 mm day^{-1}) and are warm and dry, their properties being more characteristic of suppressed MJO conditions.

b. Mixed-layer variability for full DYNAMO period

Mixed-layer depths at all three sites for the full duration of DYNAMO are shown in Fig. 8, along with time series of rainfall P_0 and precipitable water (PW). The observations at Gan extend into early February, well beyond the SOP operations at Malé and *Revelle*. The late October and late November rainy periods, roughly corresponding to MJO phases 2 and 3 based on Wheeler and Hendon (2004) index (bottom bar in Fig. 8), were associated with two MJOs that occurred during DYNAMO (Gottschalck et al. 2013; Yoneyama et al. 2013). PW at Gan and *Revelle* increased after a dry period during the first week of October, followed by the onset of rainfall and a reduction in mixed-layer depths, most notably at *Revelle*, reflecting the effects of recovering convective downdraft wakes (e.g., Fitzjarrald and Garstang 1981). The moistening and rain onset at Malé, along with reduction in mixed-layer depths, began about 1 week later as the envelope of convection from the Southern Hemisphere gradually shifted northward across the equator (Fig. 8; Johnson and Ciesielski 2013). Decreased mixed-layer depths were also observed at *Revelle* and Malé in the last half of November with the second MJO. While there is some reduction in mixed-layer depths at Gan during the MJO active phases, this behavior is not as prominent as the other sites. The reason for the lack of a distinct modulation of mixed-layer depths by the MJOs at Gan is not obvious. However, a possible explanation lies in the fact that with an enclosed lagoon, Addu Atoll represents a relatively large heat source impacting the lowest levels of the Gan soundings, hence making them less representative of open-ocean conditions and more dependent on the local diurnal cycle of heating. A prominent feature of the time series at Gan is the extended period of deeper mixed layers during the dry period in January and early February. Mean mixed-layer depths during this time were consistently greater, ~600 m, typical of undisturbed trade wind conditions (Malkus 1958; Augstein et al. 1974).

Considering that *Revelle* soundings are most representative of open-ocean conditions and that in situ flux measurements were made at that location, further analysis of the mixed-layer evolution is carried out for that site. Time series of the mixed-layer depths and companion fields based on *Revelle* data during the DYNAMO SOP are shown in Fig. 9. All curves are daily average values except z_i and SST, which are at their full measured resolution. The first 12 days of October, a suppressed MJO period over the Indian Ocean (MJO phases 6, 7, and 8), were marked by steadily increasing mixed-layer depths to over 800 m, increasing SST and near-surface (19 m) temperature T_{19m}, relatively low surface relative humidity (RH), and little rainfall

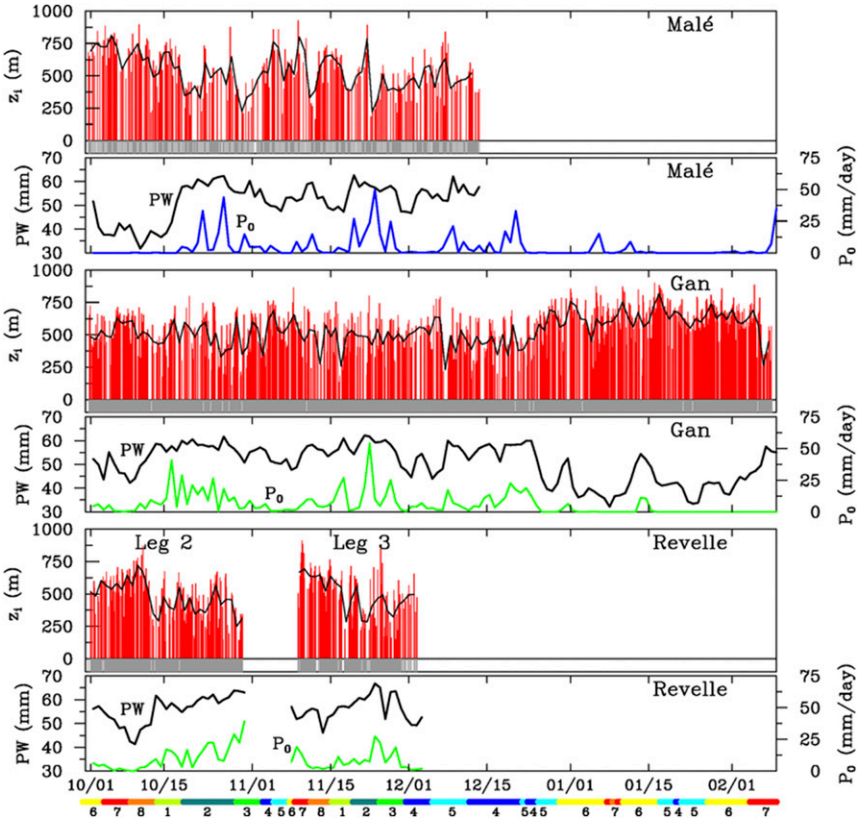

FIG. 8. Time series of mixed-layer depths (red bars) at Malé, Gan, and *Revelle* for entire period of DYNAMO sounding operations; black curves denote daily averaged values. Darker shaded region at bottom of panels indicates times at which soundings were taken. Daily average precipitation P_0: from TRMM at Malé (within a 1° radius of the island; blue curve) and from radar observations at Gan and *Revelle* (green curves); precipitable water PW from the soundings (black curves). (bottom) MJO phase based on Wheeler and Hendon (2004) index.

(Figs. 9a,c,d). SST exhibits a diurnal cycle throughout the October suppressed period despite moderate surface wind speeds of 4–6 m s^{-1} (Fig. 9b). The amplitude of the SST diurnal cycle was greater in early November owing to the lighter winds then (Ruppert and Johnson 2015). The diurnal cycle during both periods generated an afternoon maximum in shallow cumulus clouds, often organized in rolls or open-cell patterns, that played a role in lower-tropospheric moistening in the preonset stages of the MJOs (Ruppert and Johnson 2015; Rowe and Houze 2015).

Also shown in Fig. 9a is the daily averaged lifting condensation level (LCL) based on the mean thermodynamic properties of the mixed layer. During the first 12 days of October, LCL and z_i rose commensurately, with z_i reaching the LCL on a number of occasions and eventually exceeding it late in the period when the deepest mixed layers occurred. While the LCL curve represents daily averaged values and z_i is at 3-h intervals (the diurnal cycle of LCL will be examined later), the results broadly suggest that boundary layer thermals during the suppressed period can often reach the LCL and form cumulus clouds, especially toward the end of the period. This result is consistent with observations of shallow clouds being prevalent during the suppressed period, with increasing cloud amount toward the end of it (Ruppert and Johnson 2015; Rowe and Houze 2015). The *Revelle* was off station in early November at the beginning of the second suppressed period, but toward the end of this period up to about 18 November, z_i was near or greater than LCL on a number of occasions. Therefore, through the suppressed phase of both MJOs, cumulus cloud populations were aided by deeper mixed layers permitting boundary layer thermals to reach their condensation levels and promote shallow cumulus development. Since the horizontally homogeneous, steady-state mixed-layer depth over the ocean is directly proportional to the surface buoyancy flux F ($=\rho c_p \overline{w'\theta_v'}$) and inversely related to the magnitude of the large-scale subsidence (e.g., Johnson et al. 2001), the fact that F is

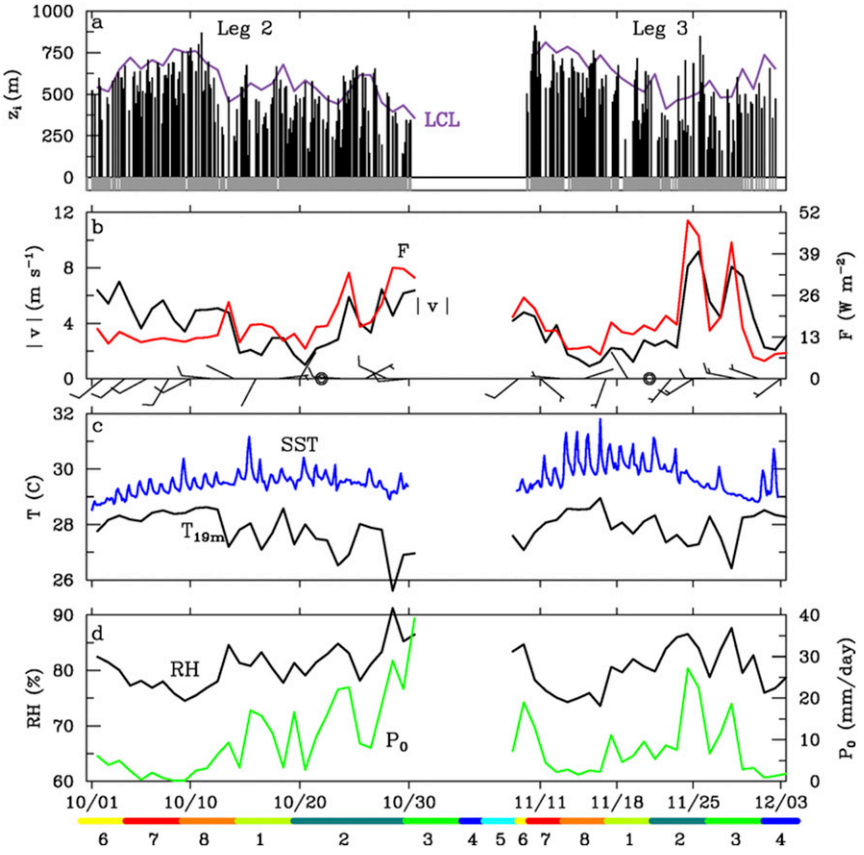

FIG. 9. Time series of (a) mixed-layer depths (black bars) during two cruises of *Revelle* (legs 2 and 3) for DYNAMO SOP along with LCL based on mixed-layer-mean conditions; (b) surface buoyancy flux F, wind speed $|\mathbf{v}|$, and surface wind plots at 6-hourly intervals; (c) SST and 19-m temperature T_{19m}; and (d) surface relative humidity (RH; adjusted to 10 m from flux tower data) and radar-estimated precipitation P_0. All curves are daily average values, except for z_i and SST, which are at their full measured resolution. Gray-shaded region in (a) indicates times at which soundings were taken. (bottom) MJO phase based on Wheeler and Hendon (2004) index.

approximately constant during the first 12 days of October suggests that the deepening mixed layers during that period could be related to a relaxation of large-scale subsidence. Powell and Houze (2015a) argued that such a situation occurred in association with the arrival of global-circumnavigating, upper-tropospheric velocity potential anomalies over the Indian Ocean. The reduction in subsidence through the suppressed phase is also consistent with results reported in Sobel et al. (2014) and Johnson et al. (2015) of decreasing net tropospheric radiative cooling rates (implying weaker large-scale subsidence) linked to gradually increasing cirrus clouds shown in the latter paper during the buildup to the active phases of both the October and November MJOs.

Surface wind speed and buoyancy flux at the *Revelle* increased significantly during the active phases of the October and November MJOs (Fig. 9b). Frequent cold pools were observed during these periods (de Szoeke et al. 2017), which contributed to the enhanced surface sensible and latent heat fluxes (Johnson et al. 2015) and the recovery of convective outflow wakes as evidenced by the numerous shallow mixed layers (Fig. 9a).

c. *Mixed-layer diurnal cycle during undisturbed conditions*

The diurnal cycle of the SST and its impact on cumulus convection were prominent features of the MJO suppressed phases during DYNAMO (Matthews et al. 2014; Ruppert and Johnson 2015). Therefore, we give attention to suppressed or undisturbed periods for the study of the mixed-layer diurnal cycle. In a previous investigation using 6-hourly COARE sounding data, a mixed-layer diurnal cycle was observed during undisturbed, light-wind conditions (Johnson et al. 2001). At R/V *Shiyan*

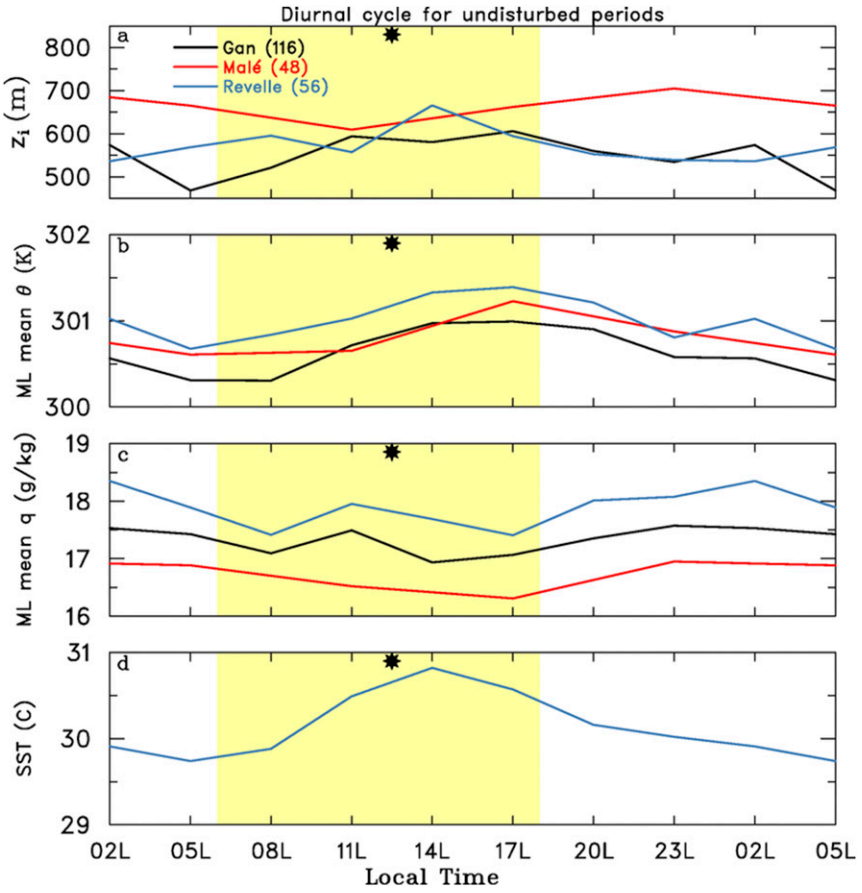

FIG. 10. Diurnal cycle of mixed-layer (a) depth (m), (b) mean potential temperature (K), and (c) mean specific humidity (g kg^{-1}) and (d) *Revelle* SST for undisturbed SOP periods. Undisturbed periods definitions—Gan: 1–10 Oct, 11–21 Nov; Malé: 3–17 Oct; *Revelle*: 11–21 Nov. Daytime denoted by yellow shading, local noon by sun symbol. Numbers of mixed-layer cases are in parentheses.

3 a diurnal cycle in SST of 1°–2°C produced a diurnal cycle in mixed-layer properties: a 60-m increase in z_i in the afternoon accompanied by a 0.5-K warming and 0.5 g kg^{-1} drying. The SST diurnal cycle at the ship was muted on disturbed days by strong winds and precipitation downdrafts. Here we report similar observations from DYNAMO, though the diurnal cycle is much better resolved with the 3-hourly soundings at Gan and *Revelle*.

Figure 10 shows SOP undisturbed mean diurnal cycle in z_i and mixed-layer mean values of θ and q at all three sounding locations, as well as SST at *Revelle*. The undisturbed periods approximately correspond to the suppressed SOP periods defined in Ruppert and Johnson (2015). All three sites show a diurnal cycle in z_i of 100–150 m peaking in the afternoon at Gan and *Revelle* and near midnight at Malé (Fig. 10a), though the timing of the true maximum for the latter site is less certain due to the 6-hourly time resolution. Each site shows an afternoon mixed-layer warming ~0.5 K and drying of ~0.5 g kg^{-1}. The warming is in part attributed to a diurnal warm layer that develops in the upper ~1 m of the ocean under light-wind, clear-sky conditions (Soloviev and Lukas 1997; Vialard et al. 2009; Moum et al. 2014), as reflected by the SST diurnal cycle shown in Figs. 9c and 10d. Enhanced surface fluxes from this upper-ocean warming served to warm the mixed layer (Fig. 10b) and contributed to an afternoon maximum in the cumulus cloud population (Ruppert and Johnson 2015, 2016). Daytime absorption of solar shortwave radiation, primarily by water vapor, has been argued to additionally contribute to daytime heating of the mixed layer (Parsons et al. 2000; Johnson et al. 2001).

Mixed-layer drying during the daytime (Fig. 10c) is partly a result of the downward entrainment of dry air from above as the mixed layer grows during the day. However, the drier conditions in the daytime may also partly be a reflection of moistening of the boundary

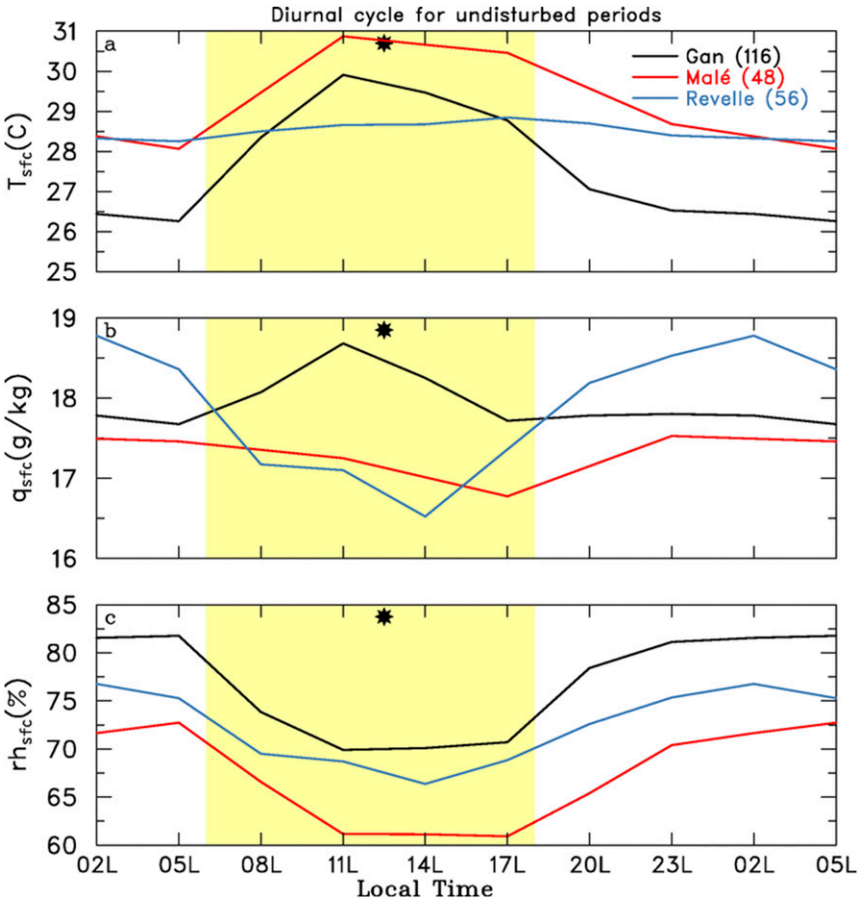

FIG. 11. As in Fig. 10, but for (a) surface temperature (°C), (b) surface specific humidity (g kg^{-1}), and (c) surface relative humidity (%) for undisturbed periods at Gan, Malé, and *Revelle*. Surface measurements at *Revelle* were at 19 m; those at Gan and Malé were at shelter height of 2 m.

layer over the equatorial oceans that occurs at night owing to radiative and/or larger-scale circulation processes (Sui et al. 1997; Bellenger et al. 2010). The mixed layer at Malé is the driest of the three sites, likely owing to its off-equatorial, Northern Hemisphere location, while *Revelle* has the highest q (Fig. 10c). The moister conditions at *Revelle* are attributed to the fact that it virtually represents open-ocean conditions. Evidence for drier conditions near the surface over land was provided in an independent study (T. Jones and H. Yamada 2011, personal communication) where near-simultaneous humidity measurements at the Malé sounding site and the adjacent ocean showed the specific humidity to be ~1 g kg^{-1} greater over water than that over land despite the small area of the island.

Additional evidence for contrasting near-surface conditions at Gan and Malé in comparison to those at *Revelle* is provided in Fig. 11. Surface temperature and humidity measurements were at 2 m at Gan and Malé and at the 19-m height of the surface meteorological sensor at *Revelle*. During the undisturbed periods, a moderate daytime surface warming of 2°–4°C was observed at Gan and Malé under the mostly clear-sky conditions, as expected at their land locations. In contrast, the 19-m temperature at *Revelle* had a relatively minor diurnal cycle, more accurately reflecting conditions over the open ocean. The diurnal cycle of near-surface specific humidity differed considerably at the three sites. *Revelle* and to a lesser extent Malé showed a midday drying, which may in part have simply been a manifestation of the nocturnal moistening, although the downward mixing of dry air from above the mixed layer may also have contributed to the drying. On the other hand, Gan exhibited a midday moistening of nearly 1 g kg^{-1}. This feature is hard to fully explain, but it may have been a consequence of the sea breeze advecting in moister air from the ocean and lagoon adjacent to Gan Island. At all three sites there was an afternoon minimum in near-surface relative humidity, which was due to the daytime surface heating at Gan

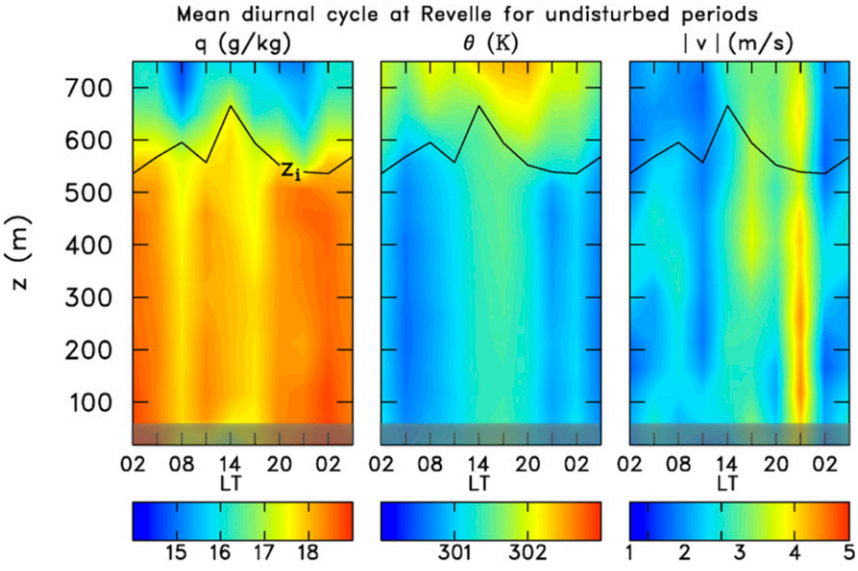

FIG. 12. Mean diurnal cycle of specific humidity q (g kg^{-1}), potential temperature θ, and wind speed (m s^{-1}) for 11–21 Nov undisturbed period at *Revelle*. Variables in each sounding are first scaled by mixed-layer depth z_i, then composited according to height relative to z_i, and finally replotted as a function of actual height z. Mixed-layer top z_i (black curve) is also shown. Values in lowest 50 m are shaded to indicate surface effects in sounding data.

and Malé but the daytime reduction in specific humidity at *Revelle*.

To further illustrate the diurnal cycle at *Revelle* under undisturbed conditions, a plot of scaled q, θ, and wind speed was created (Fig. 12). Quantities were first scaled by their height relative to the mixed-layer top at each time, scaled fields were then composited, and finally values were plotted relative to the mean mixed-layer depth at each time. The number of soundings going into the means at each time are shown in Fig. 13a.[2] Owing to the limited number of soundings in the composite, the diurnal variation of z_i (solid black curve in Fig. 12) does not exhibit a smooth diurnal cycle; that is, there was a reduction in z_i at 1100 LT on its climb to the afternoon peak at 1400 LT. Potential temperature θ and q were nearly well mixed below z_i, though there was a slight decrease in q and increase in θ near mixed-layer top. Mixed-layer warming and drying were observed in mid- to late afternoon, though there was also a drying at 0800 LT (which is also evident at Gan; Fig. 10c). This two-peak structure to the field of q, rather than there being a broad afternoon minimum, is related to the fact that there was a local minimum in the composite z_i at 1100 LT. Namely, shallower mixed layers are moister (Fig. 7), which introduced a local maximum in q at 1100 LT.

Wind speeds generally increased in the mixed layer in the afternoon (Fig. 12), as found during COARE (Johnson et al. 2001), which is a reflection of more vigorous buoyancy-driven turbulence during the daytime. Downward mixing of higher-momentum air from above the mixed layer in the afternoon was not important during this period due to the weak lower-tropospheric winds, although it does appear as a prominent feature in a composite of all 268 mixed profiles at *Revelle*, which includes many disturbed, windy days (not shown). Apart from the wind peak at 2300 LT, which represents a sampling problem [there were two anomalously windy days out of only three days in the composite at this time (Fig. 13a)], the wind speed variations (maxima at 0500 and 1700 LT and minimum at 1100 LT) in Fig. 12 are similar to those found using sounding data from COARE (Johnson et al. 2001) and are consistent with past studies of the semidiurnal and diurnal harmonics of wind profiler data for COARE (Gutzler and Hartten 1995) and of buoy data from the Pacific (Deser and Smith 1998).

A further analysis of the diurnal cycle of the mixed layer during the November undisturbed period at *Revelle* is shown in Fig. 13. During this period z_i had a diurnal range of about 130 m that accompanied a SST diurnal variation of 1 K (Figs. 13a,c). Buoyancy flux F increased in the afternoon in response to both SST and

[2] The sounding at 1100 LT 19 Nov 2011 is excluded from the composite owing to the existence of a very shallow mixed layer in a recovering convective downdraft wake following the passage of isolated showers around that time.

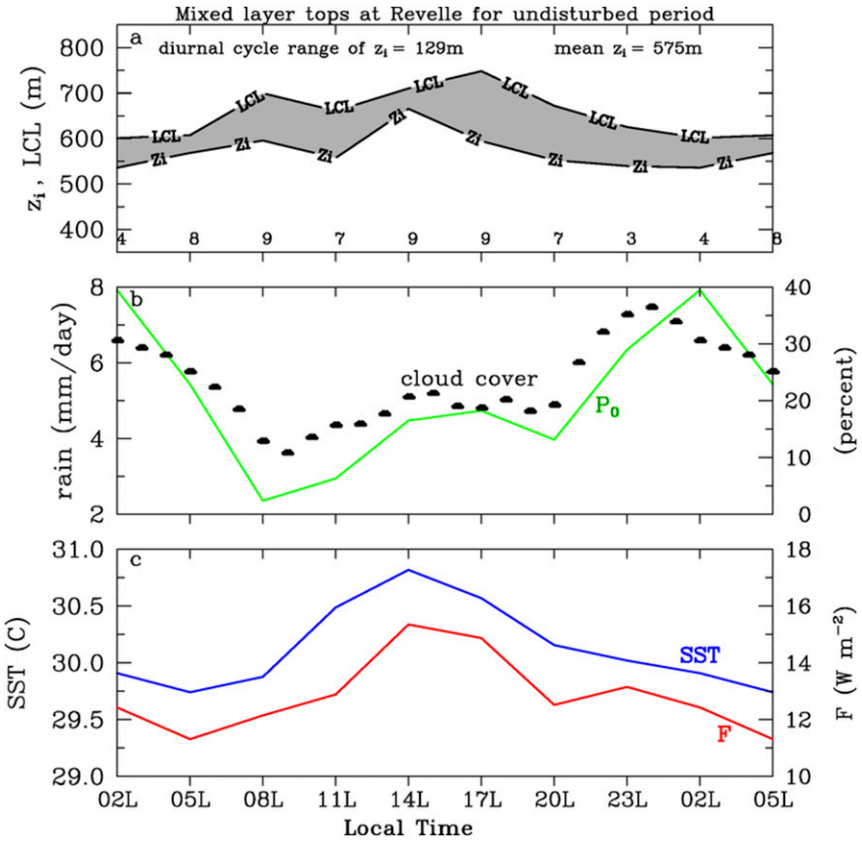

FIG. 13. (a) Diurnal cycle of mixed-layer depth z_i (m) and LCL based on mixed-layer-mean conditions, (b) mean radar-determined rainfall rate P_0 (green) in TOGA radar range and ceilometer-estimated cloud cover (cloud symbols), and (c) mean SST (blue) and surface buoyancy flux F (red) for November undisturbed period at *Revelle*. Gray shading in (a) indicates difference between LCL and z_i. Diurnal cycle range and mean value of z_i, along with numbers of soundings at each time (on bottom axis), are shown in (a).

wind speed increase, as shown by Ruppert and Johnson (2015), which directly contributed to the midday growth in z_i, as also found in COARE (Johnson et al. 2001). In response to the midday heating of the upper ocean, there were local maxima in cloud cover and rainfall (Fig. 13b), as discussed in Ruppert and Johnson (2015, 2016) and observed in previous field campaigns (Sui et al. 1997; Bellenger et al. 2010). In addition, the typical nocturnal rainfall maximum (e.g., Gray and Jacobson 1977) was present during this period despite the suppressed conditions. The two maxima in rainfall approximately coincide with the minima in LCL − z_i, which is consistent with the idea that these periods are times in which the greatest number of boundary layer thermals are able to reach their condensation levels to form clouds. This semidiurnal cycle to the cloud and precipitation occurrence is shown in Fig. 14 [adapted from Ruppert and Johnson (2015)] in terms of the S-PolKa radar echo-top height and area coverage diurnal cycle for 13–16 November, a subset of the period analyzed in Fig. 13.

4. Summary and conclusions

Atmospheric sounding data from DYNAMO are used to determine mixed-layer depths for three sites that experienced the strongest signal of the Madden–Julian oscillation during the experiment: Gan Island on Addu Atoll, Malé, and the R/V *Revelle*. Mixed layers were defined to be present when well-mixed profiles of both potential temperature θ and specific humidity q, topped by abrupt increasing stability and drying, were observed to exist and the depths determined by both profiles were within 5 hPa of each other. A number of objective techniques have been developed to determine atmospheric boundary layer (ABL) depths in the past; however, they often lead to different ABL and mixed-layer depth estimates (e.g., Liu and Liang 2010; Seidel et al.

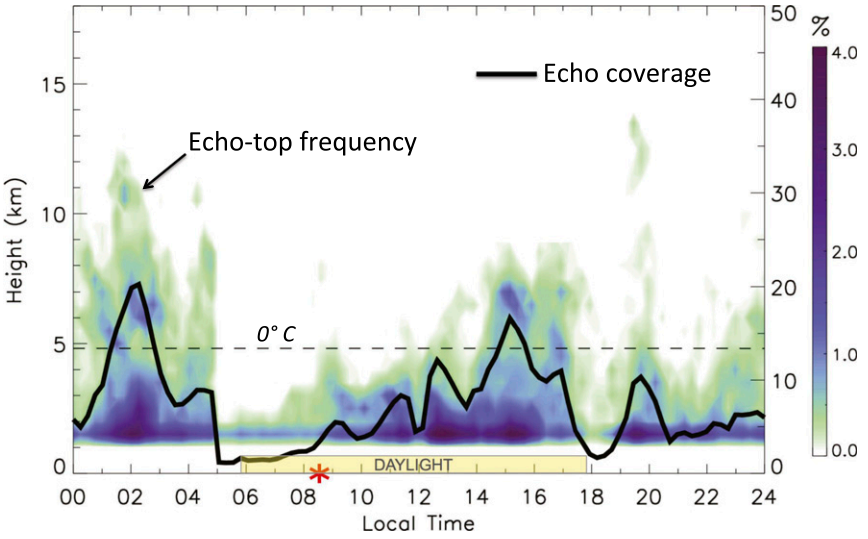

FIG. 14. Diurnal time–height composites of convective echo-top frequency (shading; %) and echo area coverage (solid black line; %; right axis) for 13–16 Nov suppressed period, calculated from 15-min S-PolKa RHI data. Local time is indicated along the abscissa. Red asterisk marks the time of increasing echo-top frequency and echo area coverage. Horizontal dashed line indicates the 0°C level. Adapted from Ruppert and Johnson (2015).

2010; Wang and Wang 2014). Recognizing these difficulties, and drawing upon experience from TOGA COARE (Johnson et al. 2001), the subjective procedure used in that study has been applied to DYNAMO sounding data for identification of mixed layers and determination of their depths and properties.

The principal findings of this study are as follows:

- Mixed layers were observed 68% of the time in DYNAMO (1220 out of 1783 soundings), which is comparable to the 72% frequency found in COARE (Johnson et al. 2001) but somewhat less than the 79% frequency determined for GATE (Fitzjarrald and Garstang 1981).
- The mean mixed-layer depth for all three sites during DYNAMO was 508 m, ranging from 491 m at *Revelle* (the rainiest site) to 535 m at Malé (the driest site). The mean value is close to that determined for COARE (512 m; Johnson et al. 2001) but is greater than the mean of 424 m determined for GATE (Fitzjarrald and Garstang 1981). Mean mixed-layer depth at Gan during a highly suppressed period in January and early February was ~600 m, which is typical of undisturbed trade wind conditions (Malkus 1958; Augstein et al. 1974).
- Mixed-layer depths ranged from a high of 926 m to a low of 111 m. Very shallow depths were often observed during the recovery of precipitation downdraft wakes, some of which lasted beyond a half day (Chen et al. 2016). The distributions of mixed-layer depths were skewed about the mean toward lower heights, reflecting the frequent presence of such wakes.
- Time series for the entire period of DYNAMO reveal a significant modulation of mixed-layer depths at Malé and *Revelle* by the October and November MJOs, but less so at Gan. During the October and November suppressed MJO periods at the Revelle, the mixed-layer depth increased as the SST increased, while large-scale subsidence decreased (Johnson and Ciesielski 2013). The decreasing subsidence may be linked to global-circumnavigating upper-tropospheric velocity potential anomalies that approached the Indian Ocean prior to the active phases of the MJOs (Gottschalck et al. 2013; Powell and Houze 2015a) as well as to a reduction in radiative heating rates caused by increasing cirrus clouds preceding the active phases (Sobel et al. 2014; Johnson et al. 2015). Frequent, shallow mixed-layer depths occurred during the active phases of the MJOs.
- A prominent diurnal cycle of the mixed-layer properties was observed at all three sites during the suppressed phases of the October and November MJOs in response to the development of an upper-ocean diurnal warm layer and resultant increase in buoyancy fluxes during relatively light-wind, and mostly clear-sky conditions. Diurnal ranges of mixed-layer depth, mixed-layer-mean θ, and mixed-layer-mean q were 100–150 m, 0.5 K, and 0.5 g kg^{-1}, respectively.
- The diurnal variation of the mixed layer and its relationship to the lifting condensation level (LCL) related

directly to the diurnal evolution of the cloud populations during suppressed periods. The afternoon deepening of the mixed layer coincided with the maximum daytime SST and led to a decrease in the distance between the LCL and the mixed-layer top. These conditions made it more likely for boundary layer thermals to reach their LCL and create clouds. This conclusion is corroborated by a gradual increase in convective radar echo-top heights peaking in midafternoon and a local rainfall maximum around that time. During predawn hours, the distance between the LCL and the mixed-layer top was similarly small, which coincided with a nocturnal peak in radar echoes and rainfall. The net result was a semidiurnal variation in precipitation during suppressed periods, consistent with findings from previous studies (Sui et al. 1997; Bellenger et al. 2010).

The results of this study bear directly on the problem of numerical simulation of the MJO, as well as global circulation modeling in general. Considering that the proper representation of the atmospheric boundary layer in weather and climate models remains a major challenge (Teixeira et al. 2008), it is important to obtain observations of the boundary layer to validate models. With respect to the MJO itself, Qian et al. (2016) found large sensitivities in the simulation of the MJO using different boundary layer parameterizations in the Weather Research and Forecasting (WRF) Model. Cumulus clouds have their roots in the mixed layer, so simulating realistic mixed-layer depth and properties is a logical prerequisite for realistic simulations of cloud populations and their precipitation. This paper is intended to provide analyses that can be used for this purpose.

Acknowledgments. We appreciate the valuable comments of three reviewers, which have led to significant improvements to the paper. We also thank Jennifer Davison in connection with our early collaborations with her on this work. This research has been supported by the National Science Foundation under Grant AGS-1360237 and by the National Oceanic and Atmospheric Administration (NOAA) under Grant NA150AR4310177.

REFERENCES

Augstein, E., H. Schmidt, and F. Ostapoff, 1974: The vertical structure of the atmospheric planetary boundary layer in undisturbed trade winds over the Atlantic Ocean. *Bound.-Layer Meteor.*, **6**, 129–150.

Baranowski, D. B., M. K. Flatau, P. J. Flatau, and A. J. Matthews, 2016: Impact of atmospheric convectively coupled equatorial Kelvin waves on upper ocean variability. *J. Geophys. Res. Atmos.*, **121**, 2045–2059, doi:10.1002/2015JD024150.

Barnes, G. M., and M. Garstang, 1982: Subcloud layer energetics of precipitating convection. *Mon. Wea. Rev.*, **110**, 102–117, doi:10.1175/1520-0493(1982)110<0102:SLEOPC>2.0.CO;2.

Bellenger, H., Y. N. Takayabu, T. Ushiyama, and K. Yoneyama, 2010: Role of diurnal warm layers in the diurnal cycle of convection over the tropical Indian Ocean during MISMO. *Mon. Wea. Rev.*, **138**, 2426–2433, doi:10.1175/2010MWR3249.1.

——, K. Yoneyama, M. Katsumata, T. Nishizawa, K. Yasunaga, and R. Shirooka, 2015: Observation of moisture tendencies related to shallow convection. *J. Atmos. Sci.*, **72**, 641–659, doi:10.1175/JAS-D-14-0042.1.

Chen, S., and Coauthors, 2015: A study of CINDY/DYNAMO MJO suppressed phase. *J. Atmos. Sci.*, **72**, 3755–3779, doi:10.1175/JAS-D-13-0348.1.

Chen, S. S., and Coauthors, 2016: Aircraft observations of dry air, the ITCZ, convective cloud systems, and cold pools in MJO during DYNAMO. *Bull. Amer. Meteor. Soc.*, **97**, 405–423, doi:10.1175/BAMS-D-13-00196.1.

Ciesielski, P. E., and Coauthors, 2014: Quality-controlled upper-air sounding dataset for DYNAMO/CINDY/AMIE: Development and corrections. *J. Atmos. Oceanic Technol.*, **31**, 741–764, doi:10.1175/JTECH-D-13-00165.1.

Deser, C., and C. A. Smith, 1998: Diurnal and semidiurnal variations of the surface wind field over the tropical Pacific Ocean. *J. Climate*, **11**, 1730–1748, doi:10.1175/1520-0442(1998)011<1730:DASVOT>2.0.CO;2.

de Szoeke, S. P., J. B. Edson, J. R. Marion, C. W. Fairall, and L. Bariteau, 2015: The MJO and air–sea interaction in TOGA COARE and DYNAMO. *J. Climate*, **28**, 597–622, doi:10.1175/JCLI-D-14-00477.1.

——, E. D. Skyllingstad, P. Zuidema, and A. S. Chandra, 2017: Cold pools and their influence on the tropical marine boundary layer. *J. Atmos. Sci.*, **74**, 1149–1168, doi:10.1175/JAS-D-16-0264.1.

Fairall, C. W., E. F. Bradley, J. E. Hare, A. A. Grachev, and J. B. Edson, 2003: Bulk parameterization of air–sea fluxes: Updates and verification for the COARE algorithm. *J. Climate*, **16**, 571–591, doi:10.1175/1520-0442(2003)016<0571:BPOASF>2.0.CO;2.

Feng, Z., S. Hagos, A. K. Rowe, C. D. Burleyson, M. N. Martini, and S. P. de Szoeke, 2015: Mechanism of convective cloud organization by cold pools over tropical warm ocean during the AMIE/DYNAMO field campaign. *J. Adv. Model. Earth Syst.*, **7**, 357–381, doi:10.1002/2014MS000384.

Fitzjarrald, D. R., and M. Garstang, 1981: Vertical structure of the tropical boundary layer. *Mon. Wea. Rev.*, **109**, 1512–1526, doi:10.1175/1520-0493(1981)109<1512:VSOTTB>2.0.CO;2.

Gottschalck, J., P. E. Roundy, C. J. Schreck III, A. Vintzileos, and C. Zhang, 2013: Large-scale atmospheric and oceanic conditions during the 2011–12 DYNAMO field campaign. *Mon. Wea. Rev.*, **141**, 4173–4196, doi:10.1175/MWR-D-13-00022.1.

Gray, W. M., and R. W. Jacobson Jr., 1977: Diurnal variation of deep cumulus convection. *Mon. Wea. Rev.*, **105**, 1171–1188, doi:10.1175/1520-0493(1977)105<1171:DVODCC>2.0.CO;2.

Gutzler, D. S., and L. M. Hartten, 1995: Daily variability of lower tropospheric winds over the tropical western Pacific. *J. Geophys. Res.*, **100**, 22 999–23 008, doi:10.1029/95JD01879.

Houze, R. A., Jr., 1977: Structure and dynamics of a tropical squall–line system. *Mon. Wea. Rev.*, **105**, 1540–1567, doi:10.1175/1520-0493(1977)105<1540:SADOAT>2.0.CO;2.

Huffman, G. J., R. F. Adler, D. T. Bolvin, G. Gu, E. J. Nelkin, K. P. Bowman, E. F. Stocker, and D. B. Wolff, 2007: The TRMM Multisatellite Precipitation Analysis: Quasi-global, multiyear, combined-sensor precipitation estimates at fine scales. *J. Hydrometeor.*, **8**, 38–55, doi:10.1175/JHM560.1.

Johnson, R. H., and M. E. Nicholls, 1983: A composite analysis of the boundary layer accompanying a tropical squall line. *Mon. Wea. Rev.*, **111**, 308–319, doi:10.1175/1520-0493(1983)111<0308:ACAOTB>2.0.CO;2.

——, and X. Lin, 1997: Episodic trade wind regimes over the western Pacific warm pool. *J. Atmos. Sci.*, **54**, 2020–2034, doi:10.1175/1520-0469(1997)054<2020:ETWROT>2.0.CO;2.

——, and P. E. Ciesielski, 2000: Rainfall and radiative heating rate estimates from TOGA COARE atmospheric budgets. *J. Atmos. Sci.*, **57**, 1497–1514, doi:10.1175/1520-0469(2000)057<1497:RARHRF>2.0.CO;2.

——, and ——, 2013: Structure and properties of Madden–Julian oscillations deduced from DYNAMO sounding arrays. *J. Atmos. Sci.*, **70**, 3157–3179, doi:10.1175/JAS-D-13-065.1.

——, ——, and J. A. Cotturone, 2001: Multiscale variability of the atmospheric mixed layer over the western Pacific warm pool. *J. Atmos. Sci.*, **58**, 2729–2750, doi:10.1175/1520-0469(2001)058<2729:MVOTAM>2.0.CO;2.

——, ——, J. H. Ruppert Jr., and M. Katsumata, 2015: Sounding-based thermodynamic budgets for DYNAMO. *J. Atmos. Sci.*, **72**, 598–622, doi:10.1175/JAS-D-14-0202.1.

Jorgensen, D. P., M. A. LeMone, and S. B. Trier, 1997: Structure and evolution of the 22 February 1993 TOGA COARE squall line: Aircraft observations of precipitation, circulation, and surface energy fluxes. *J. Atmos. Sci.*, **54**, 1961–1985, doi:10.1175/1520-0469(1997)054<1961:SAEOTF>2.0.CO;2.

LeMone, M. A., and W. T. Pennell, 1976: The relationship of trade wind cumulus distribution to subcloud layer fluxes and structure. *Mon. Wea. Rev.*, **104**, 524–539, doi:10.1175/1520-0493(1976)104<0524:TROTWC>2.0.CO;2.

Liu, S., and X.-Z. Liang, 2010: Observed diurnal cycle climatology of planetary boundary layer height. *J. Climate*, **23**, 5790–5809, doi:10.1175/2010JCLI3552.1.

Malkus, J. S., 1958: On the structure of the trade wind moist layer. MIT and WHOI Papers in Physical Oceanography and Meteorology, Vol. 13, No. 2, 47 pp., doi:10.1575/1912/1065.

——, and M. E. Stern, 1953: The flow of a stable atmosphere over a heated island, part 1. *J. Meteor.*, **10**, 30–41, doi:10.1175/1520-0469(1953)010<0030:TFOASA>2.0.CO;2.

Matthews, A. J., D. B. Baranowski, K. J. Heywood, P. J. Flatau, and S. Schmidtko, 2014: The surface diurnal warm layer in the Indian Ocean during CINDY/DYNAMO. *J. Climate*, **27**, 9101–9122, doi:10.1175/JCLI-D-14-00222.1.

Moum, J. N., and Coauthors, 2014: Air–sea interactions from westerly wind bursts during the November 2011 MJO in the Indian Ocean. *Bull. Amer. Meteor. Soc.*, **95**, 1185–1199, doi:10.1175/BAMS-D-12-00225.1.

Nicholls, S., and M. A. LeMone, 1980: The fair weather boundary layer in GATE: The relationship of subcloud fluxes and structure to the distribution and enhancement of cumulus clouds. *J. Atmos. Sci.*, **37**, 2051–2067, doi:10.1175/1520-0469(1980)037<2051:TFWBLI>2.0.CO;2.

Parsons, D. B., J.-L. Redelsperger, and K. Yoneyama, 2000: The evolution of the tropical western Pacific atmosphere-ocean system following the arrival of a dry intrusion. *Quart. J. Roy. Meteor. Soc.*, **126**, 517–548, doi:10.1002/qj.49712656307.

Powell, S. W., and R. A. Houze, 2013: The cloud population and onset of the Madden-Julian Oscillation over the Indian Ocean during DYNAMO-AMIE. *J. Geophys. Res. Atmos.*, **118**, 11 979–11 995, doi:10.1002/2013JD020421.

——, and ——, 2015a: Effect of dry large-scale vertical motions on initial MJO convective onset. *J. Geophys. Res. Atmos.*, **120**, 4783–4805, doi:10.1002/2014JD022961.

——, and R. A. Houze Jr., 2015b: Evolution of precipitation and convective echo top heights observed by TRMM radar over the Indian Ocean during DYNAMO. *J. Geophys. Res. Atmos.*, **120**, 3906–3919, doi:10.1002/2014JD022934.

Qian, Y., H. Yan, L. K. Berg, S. Hagos, Z. Feng, B. Yang, and M. Huang, 2016: Assessing impacts of PBL and surface layer schemes in simulating the surface–atmosphere interactions and precipitation over the tropical ocean using observations from AMIE/DYNAMO. *J. Climate*, **29**, 8191–8210, doi:10.1175/JCLI-D-16-0040.1.

Rowe, A. K., and R. A. Houze Jr., 2015: Cloud organization and growth during the transition from suppressed to active MJO conditions. *J. Geophys. Res. Atmos.*, **120**, 10 324–10 350, doi:10.1002/2014JD022948.

Ruppert, J. H., Jr., and R. H. Johnson, 2015: Diurnally modulated cumulus moistening in the preonset stage of the Madden–Julian oscillation during DYNAMO. *J. Atmos. Sci.*, **72**, 1622–1647, doi:10.1175/JAS-D-14-0218.1.

——, and ——, 2016: On the cumulus diurnal cycle over the tropical warm pool. *J. Adv. Model. Earth Syst.*, **8**, 669–690, doi:10.1002/2015MS000610.

Saxen, T. R., and S. A. Rutledge, 1998: Surface fluxes and boundary layer recovery in TOGA COARE: Sensitivity to convective organization. *J. Atmos. Sci.*, **55**, 2763–2781, doi:10.1175/1520-0469(1998)055<2763:SFABLR>2.0.CO;2.

Seidel, D. J., C. O. Ao, and K. Li, 2010: Estimating climatological planetary boundary layer heights from radiosonde observations: Comparison of methods and uncertainty analysis. *J. Geophys. Res.*, **115**, D16113, doi:10.1029/2009JD013680.

Seo, H., A. C. Subramanian, A. J. Miller, and N. R. Cavanaugh, 2014: Coupled impacts of the diurnal cycle of sea surface temperature on the Madden–Julian oscillation. *J. Climate*, **27**, 8422–8443, doi:10.1175/JCLI-D-14-00141.1.

Sobel, A., S. Wang, and D. Kim, 2014: Moist static energy budget of the MJO during DYNAMO. *J. Atmos. Sci.*, **71**, 4276–4291, doi:10.1175/JAS-D-14-0052.1.

Soloviev, A., and R. Lukas, 1997: Observation of large diurnal warming events in the near-surface layer of the western equatorial Pacific warm pool. *Deep-Sea Res. I*, **44**, 1055–1076, doi:10.1016/S0967-0637(96)00124-0.

Sui, C.-H., K.-M. Lau, Y. N. Takayabu, and D. A. Short, 1997: Diurnal variations in tropical oceanic cumulus convection during TOGA COARE. *J. Atmos. Sci.*, **54**, 639–655, doi:10.1175/1520-0469(1997)054<0639:DVITOC>2.0.CO;2.

Teixeira, J., and Coauthors, 2008: Parameterization of the atmospheric boundary layer: A view from just above the inversion. *Bull. Amer. Meteor. Soc.*, **89**, 453–458, doi:10.1175/BAMS-89-4-453.

Vialard, J., and Coauthors, 2009: Cirene: Air–sea interactions in the Seychelles–Chagos thermocline ridge region. *Bull. Amer. Meteor. Soc.*, **90**, 45–61, doi:10.1175/2008BAMS2499.1.

Wang, X. Y., and K. C. Wang, 2014: Estimation of atmospheric mixing layer height from radiosonde data. *Atmos. Meas. Tech.*, **7**, 1701–1709, doi:10.5194/amt-7-1701-2014.

Wheeler, M. C., and H. H. Hendon, 2004: An all-season real-time multivariate MJO index: Development of an index for monitoring and prediction. *Mon. Wea. Rev.*, **132**, 1917–1932, doi:10.1175/1520-0493(2004)132<1917:AARMMI>2.0.CO;2.

Xu, W., and S. A. Rutledge, 2014: Convective characteristics of the Madden–Julian oscillation over the central Indian Ocean observed by shipborne radar during DYNAMO. *J. Atmos. Sci.*, **71**, 2859–2877, doi:10.1175/JAS-D-13-0372.1.

Yoneyama, K., C. Zhang, and C. N. Long, 2013: Tracking pulses of the Madden–Julian oscillation. *Bull. Amer. Meteor. Soc.*, **94**, 1871–1891, doi:10.1175/BAMS-D-12-00157.1.

Young, G. S., S. M. Perugini, and C. W. Fairall, 1995: Convective wakes in the equatorial western Pacific during TOGA. *Mon. Wea. Rev.*, **123**, 110–123, doi:10.1175/1520-0493(1995)123<0110:CWITEW>2.0.CO;2.

Yuter, S. E., and R. A. Houze Jr., 1995: Three-dimensional kinematic and microphysical evolution of Florida cumulonimbus. Part II: Frequency distributions of vertical velocity, reflectivity, and differential reflectivity. *Mon. Wea. Rev.*, **123**, 1941–1963, doi:10.1175/1520-0493(1995)123<1941:TDKAME>2.0.CO;2.

Zhang, C., J. Gottschalck, E. D. Maloney, M. W. Moncrieff, F. Vitart, D. E. Waliser, B. Wang, and M. C. Wheeler, 2013: Cracking the MJO nut. *Geophys. Res. Lett.*, **40**, 1223–1230, doi:10.1002/grl.50244.

Zipser, E. J., 1977: Mesoscale and convective-scale downdrafts as distinct components of squall-line circulation. *Mon. Wea. Rev.*, **105**, 1568–1589, doi:10.1175/1520-0493(1977)105<1568:MACDAD>2.0.CO;2.

Zuidema, P., and Coauthors, 2012: On trade wind cumulus cold pools. *J. Atmos. Sci.*, **69**, 258–280, doi:10.1175/JAS-D-11-0143.1.